Computational Study on the Kinetics and Mechanism for the Unimolecular Decomposition of $C_6H_5NO_2$ and the Related $C_6H_5 + NO_2$ and $C_6H_5O + NO$ Reactions†

Shucheng Xu‡ and M. C. Lin*

Department of Chemistry, Emory University, Atlanta, Georgia 30322

Received: July 26, 2004; In Final Form: January 21, 2005

The kinetics and mechanisms for the unimolecular dissociation of nitrobenzene and related association reactions $C_6H_5 + NO_2$ and $C_6H_5O + NO$ have been studied computationally at the G2M(RCC, MP2) level of theory in conjunction with rate constant prediction with multichannel RRKM calculations. Formation of $C_6H_5 + NO_2$ was found to be dominant above 850 K with its branching ratio > 0.78, whereas the formation of $C_6H_5O + NO$ via the C_6H_5ONO intermediate was found to be competitive at lower temperatures, with its branching ratio increasing from 0.22 at 850 K to 0.97 at 500 K. The third energetically accessible channel producing $C_6H_4 + HONO$ was found to be uncompetitive throughout the temperature range investigated, 500−2000 K. The predicted rate constants for $C_6H_5NO_2 \rightarrow C_6H_5 + NO_2$ and $C_6H_5O + NO \rightarrow C_6H_5ONO$ under varying experimental conditions were found to be in good agreement with all existing experimental data. For $C_6H_5 + NO_2$, the combination processes producing C_6H_5ONO and $C_6H_5NO_2$ are dominant at low temperature and high pressure, while the disproportionation process giving $C_6H_5O + NO$ via C_6H_5ONO becomes competitive at low pressure and dominant at temperatures above 1000 K.

Introduction

Nitrobenzene ($C_6H_5NO_2$) is a prototypical molecule for studies of the kinetics of combustion and decomposition of energetic materials. The decomposition of nitrobenzene has been studied by pyrolysis using different heating methods. Matveev et al.[1] investigated the kinetics with a static cell in temperature range 683−753 K at 8−383 Torr of pure nitrobenzene and reported the first-order rate constant $k_1 = 2.09 \times 10^{17}$ exp[−(35900 ± 716)/*T*] s^{-1}. Gonzalez et al.[2] measured the rate constant in temperature range 1110−1250 K in 110 Torr SF_6 bath gas using laser-powered homogeneous pyrolysis; they obtained $k_1 = 3.16 \times 10^{15}$ exp [−(35200 ± 702)/*T*] s^{-1}. Tsang and co-workers[3] studied the decomposition kinetics in the temperature range 1070−1180 K at 1824−3344 Torr Ar pressure using a single-pulse shock-tube; they gave the first-order rate constant, $k_1 = 1.9 \times 10^{15}$ exp[−33700/*T*] s^{-1}. In the latter two studies, the kinetics for the unimolecular decomposition of cyclohexene and 1,2-dimethyl-cyclohexene were employed as internal temperature standards, respectively.

The dynamics of nitrobenzene photodissociation reaction has also been studied using different techniques.[4−10] Three primary dissociation pathways have been observed at wavelengths between 220 and 280 nm, producing $C_6H_5 + NO_2$, $C_6H_5NO + O$, and $C_6H_5O + NO$.[9,10] Theoretically, the geometries and energies of nitrobenzene in the ground state, and singlet and triplet excited states have been calculated by CAS−SCF method;[11] its isomerization to phenylnitrite has been predicted by the MP2(FC)/6-31G(d) method;[12] and the structures of some nitrobenzene isomers were optimized at the B3LYP/6-31+G-(d, p) level.[13] The energies for its dissociation to $C_6H_5 + NO_2$[13] and $C_6H_5O + NO$[8,13] have also been computed at the B3LYP/6-31G(d) level[8] and the B3LYP/6-31+G(d,p) level.[13] The related association of the phenoxy radical with NO has been investigated with several experimental techniques and the rate constants for $C_6H_5O + NO \rightarrow C_6H_5ONO$ have been reported for the temperature range 280−373 K.[14−16]

In present work, the kinetics and mechanism for the isomerization and decomposition of nitrobenzene have been computationally studied at the G2M(RCC, MP2) level of theory.[16] The potential energy surface (PES) and rate constants for various individual product channels including their related association processes, $C_6H_5 + NO_2$ and $C_6H_5O + NO$, have been predicted and the results are reported herein for high-temperature combustion modeling applications.

Computational Method

The optimized geometries of nitrobenzene, eight stable isomers, 11 transition states, and products for the four dissociation channels have been calculated at the B3LYP/6-311G(d, p) level. To obtain more reliable values of energies for potential energy surface (PES) and rate constant predictions, we performed a series of single-point energy calculations for each molecule and transition state with the G2M(RCC, MP2) scheme[17] based on the optimized geometries at the B3LYP/6-311G(d, p) level.

The G2M (RCC, MP2) composite scheme is given as follows:

$$E_0[\text{G2M}] = \text{RCCSD(T)/6-311G(d, p)} + \text{MP2/6-311+G(3df,2p)} - \text{MP2/6-311G(d, p)} + \Delta\text{HLC} + \text{ZPE}$$

The higher level correction (ΔHLC) is given by $-5.3n_\beta - 0.19n_\alpha$ in millihartree, where n_α and n_β are the numbers of α and β valence electrons, respectively. Nitrobenzene and the products of the four dissociation channels have also been

† Part of the special issue "George W. Flynn Festschrift".

* Corresponding author. E-mail: chemmcl@emory.edu. NSC Distinguished Visiting Professor at NCTU.

‡ Cherry L. Emerson Visiting Fellow in Cherry L. Emerson Center for Scientific Computation, Emory University. E-mail: sxu@emory.edu.

10.1021/jp046688+ CCC: $30.25
Published on Web 03/02/2005

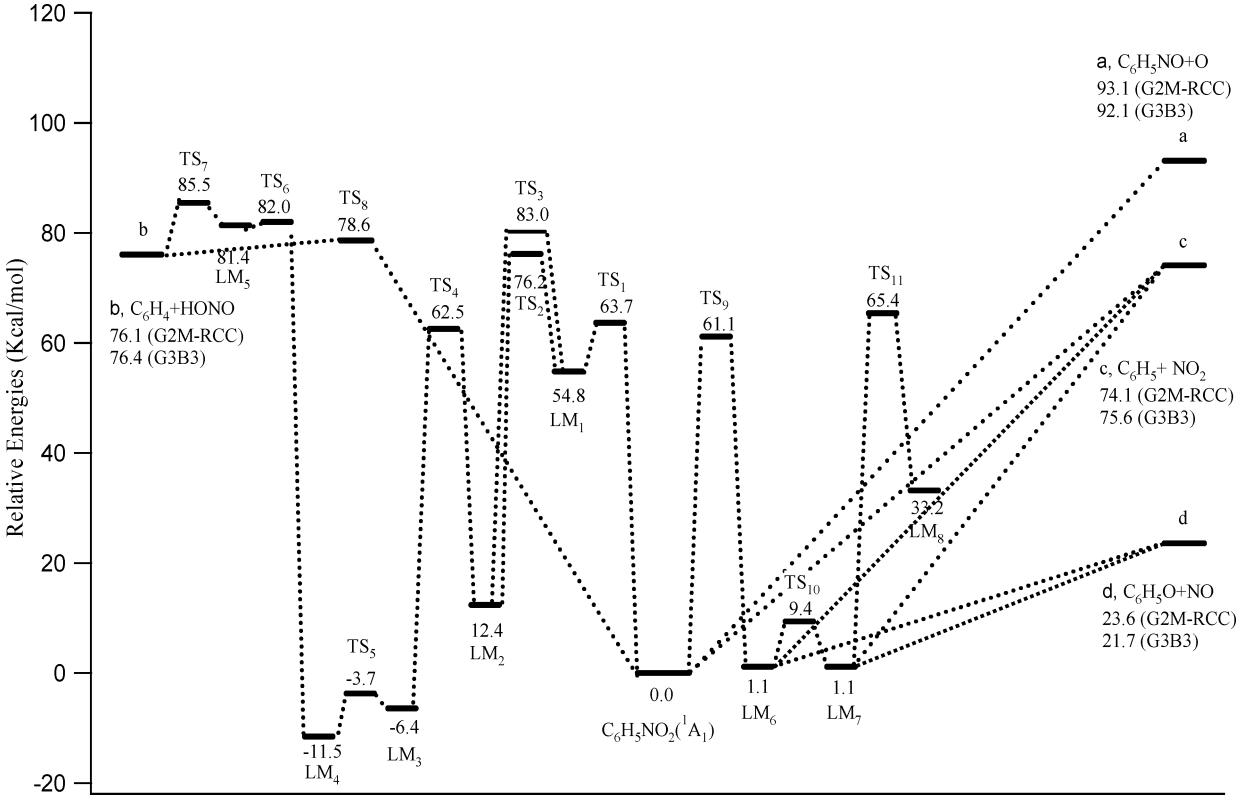

Figure 1. Schematic energy diagram for the isomerization and dissociation reactions of $C_6H_5NO_2$ calculated at the G2M(RCC, MP2)//B3LYP/6-311G(d, p) level with some calculated at the G3B3//B3LYP/6-31G(d) level, where energy units in kcal per mole.

calculated by the G3B3 composite method[18] with the geometries optimized at the B3LYP/6-31+G(d) level.

All calculations were carried out by the Gaussian 03[19] and MOLPRO 98 programs[20] using a PC cluster and the computers at Cherry L. Emerson Center for Scientific Computation at Emory University.

Results and Discussion

1. Isomerization of Nitrobenzene. The energy diagram of the $C_6H_5NO_2$ system, including various isomerization and decomposition reactions, computed with the G2M (RCC, MP2) method[17] is shown in Figure 1. The relative energies using the B3LYP/6-311G(d, p), MP2/6-311G(d, p), MP2/6-311+G(3df, 2p), RCCSD(T)/6-311G(d, p), G2M (RCC, MP2), and G3B3 methods are also listed in Table 1. The optimized structures of the nitrobenzene (S_0), its eight isomers (LM_{1-8}), and 11 transition states (TS_{1-11}) are presented in Figure 2. The geometry of $C_6H_5NO_2$ in the ground S_0 state is a planar structure with C_{2v} symmetry. Among the 8 isomers, LM_3, LM_4, and LM_5 are planar structures with C_s symmetry; LM_3 and LM_4 are two conformations of 2-nitrosophenol, $C_6H_4(OH)NO$, which are the most stable structures among the isomers. LM_6 and LM_7 are two conformations of C_6H_5ONO (phenylnitrite or nitritobenzene), which is an important intermediate for the dissociation process, $C_6H_5NO_2 \rightarrow C_6H_5O + NO$, particularly at low temperatures (vide infra). As illustrated in Figure 1, nitrobenzene and its isomers can transform into each other by numerous isomerization reactions: S_0 isomerizes to LM_1 by TS_1 with a 63.7 kcal/mol barrier; LM_1 to LM_2 by TS_2 or TS_3 with a 21.4 or 28.2 kcal/mol barrier; LM_2 to LM_3 by TS_4 with a 50.1 kcal/mol barrier; LM_3 to LM_4 by TS_5 with a small torsional barrier of 2.7 kcal/mol; LM_4 to LM_5 by TS_6 with a large OH-migration barrier, 93.5 kcal/mol. Furthermore, S_0 can also isomerize over a 61.1 kcal/mol barrier at TS_9 to LM_6 (phenylnitrite with a CONO trans-structure) which can torsionally isomerize to its cis-counterpart (LM_7) by TS_{10} with a barrier of 8.3 kcal/mol. LM_7 can isomerize to LM_8 by TS_{11} with a 64.3 kcal/mol barrier. Polasek et al.[13] also optimized the geometries of nitrobenzene isomers including S_0, LM_5, LM_6, and LM_7 in this work at the B3LYP/6-31+G(d, p) level. Most of the isomerization reactions, except the formation of phenylnitrite, which decomposes readily into $C_6H_5 + NO_2$ and $C_6H_5O + NO$, are irrelevant to the decomposition processes discussed below.

2. Dissociation of Nitrobenzene. 2a. $C_6H_5NO_2 \rightarrow C_6H_5 + NO_2$. This pathway is the primary channel for the photodissociation of $C_6H_5NO_2$.[9,10] The predicted dissociation energy is 74.1 kcal/mol using the G2M method and 75.6 kcal/mol based on the G3B3 method. These values are close to the experimental heat of reaction at 0 K, 71.9 ± 0.9 kcal/mol, based on $\Delta_f H_0(C_6H_5NO_2) = 20.95 \pm 0.12$ kcal/mol using $\Delta_f H_{298}(C_6H_5NO_2) = 16.13 \pm 0.12$ kcal/mol,[21] $\Delta_f H_0(NO_2) = 8.59 \pm 0.19$ kcal/mol,[21] and $\Delta_f H_0(C_6H_5) = 84.3 \pm 0.6$ kcal/mol.[22] There are two possible channels for this reaction: the main channel is the direct dissociation process occurring by breaking the C−N bond without an intrinsic transition state; the second channel takes place first by isomerization to C_6H_5ONO with a barrier of 61.1 kcal/mol at TS_9 as mentioned above. Its two conformers LM_6 and LM_7, can dissociate to $C_6H_5 + NO_2$ by breaking the C−O bond, also without an intrinsic barrier. However, the second channel contributes negligibly because of the tight transition state TS_9 and of the competitively low energy for formation of $C_6H_5O + NO$ (50.5 kcal/mol vs74.1 kcal/mol for $C_6H_5 + NO_2$).

2b. $C_6H_5NO_2 \rightarrow C_6H_5O + NO$. As alluded to above, this dissociation pathway takes place first by isomerization to C_6H_5ONO via TS_9, followed by dissociation to $C_6H_5O + NO$ from its two conformers, LM_6 and LM_7. The rate-controlling barrier at TS_9 is 61.1 kcal/mol. Tsang et al.[3] found this to be one of

TABLE 1: Relative Energies[a] for the Isomerization, Transition States, and Dissociation Reactions of $C_6H_5NO_2$

species or reactions	ΔZPE	B3LYP/ 6-311G(d,p)	MP2/ 6-311G(d,p)	MP2/ 6-311+G(3df,2p)	RCCSD(T)/ 6-311G(d, p)	G2M[b]	G3B3[c]	expt
S_0	0.0	0.0	0.0	0.0	0.0	0.0	0.0	
LM_1	−0.9	59.2	61.3	59.2	57.9	54.8		
LM_2	−2.2	14.5	20.4	24.5	10.6	12.4		
LM_3	−1.0	−5.0	−2.5	−0.9	−7.0	−6.4		
LM_4	−0.4	−11.9	−9.1	−7.2	−13.0	−11.5		
LM_5	−1.8	79.6	90.2	89.5	83.9	81.4		
LM_6	−1.7	0.5	4.3	6.7	−0.2	1.1		
LM_7	−1.7	1.7	5.0	7.0	0.9	1.1		
LM_8	−1.9	41.3	41.1	42.6	33.6	33.2		
TS_1	−1.5	64.4	70.2	67.4	68.1	63.7		
TS_2	−4.6	78.0	100.3	98.0	83.0	76.2		
TS_3	−3.9	81.2	107.8	104.8	89.8	83.0		
TS_4	−5.4	61.0	71.7	73.6	66.0	62.5		
TS_5	−1.8	−1.6	0.7	2.4	−3.8	−3.7		
TS_6	−3.8	98.4	121.2	119.3	87.7	82.0		
TS_7	−2.7	84.5	95.4	95.6	88.0	85.5		
TS_8	−3.6	78.6	85.8	87.6	80.4	78.6		
TS_9	−2.9	62.8	65.6	64.0	65.6	61.2		
TS_{10}	−2.4	10.3	13.0	15.6	9.2	9.4		
TS_{11}	−3.7	69.1	87.2	85.4	70.9	65.4		
$C_6H_5 + NO_2$	−3.6	66.3	103.7	105.8	73.2	74.1	75.6	(71.9 ± 0.9) [d]
$C_6H_5O + NO$	−4.5	15.1	53.4	61.0	17.4	23.6	21.7	(20.0 ± 1.9)[e]
$C_6H_4 + HONO$	−4.4	79.1	82.9	85.0	78.7	76.1	76.4	(72.4 ± 5.0)[d]
$C_6H_5NO + O$	−4.8	88.9	93.6	104.7	82.9	93.1	92.1	(89.6 ± 1.3)[d]

[a] Relative energies are ZPE-corrected in kcal mol^{-1}. [b] On the basis of the optimized geometries calculated at B3LYP/6-311G(d,p). [c] On the basis of the optimized geometries calculated at B3LYP/6-31+G(d). [d] The data from derived heat formation of the reaction at 0 K. [e] The bond dissociation energy at 0 *K* of phenoxy−NO relative to nitrobenzene from ref 15.

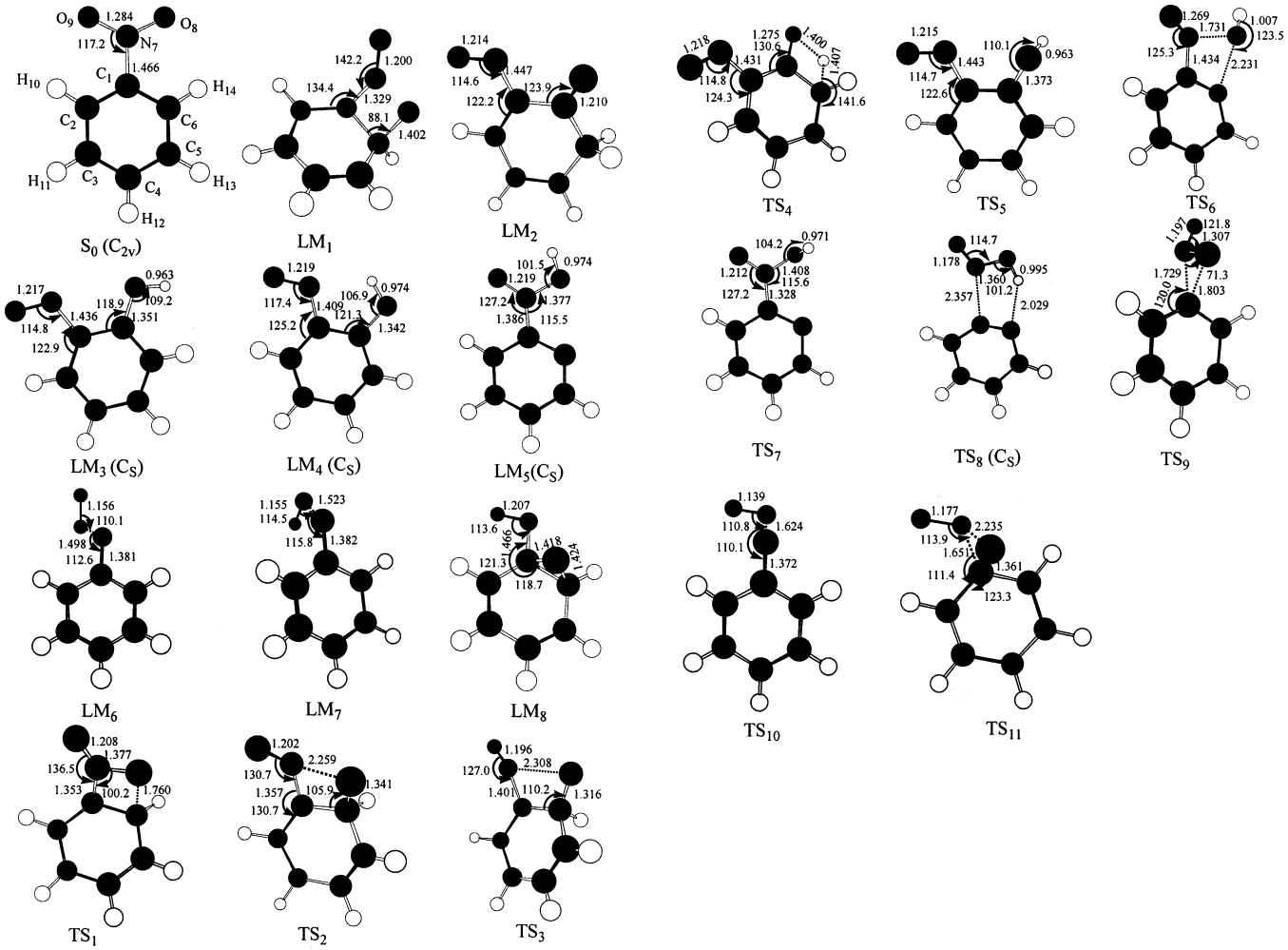

Figure 2. Optimized geometries of nitrobenzene (S_0), 8 isomers (LM_1 to LM_8) and 11 transition states (TS_1 to TS_{11}) for the isomerization and dissociation reactions of $C_6H_5NO_2$ calculated at the B3LYP/6-311G(d, p) level.

the important initial key processes in the thermal decomposition of nitrobenzene based on their shock-tube experiment. In their photodissociation study, Galloway et al.[10] concluded that the decomposition occurred by the isomerization from an excited state to phenylnitrite, which then produces NO by cleaving the C_6H_5O-NO bond. They also calculated the equilibrium geometry of C_6H_5ONO using PM2/6-31G(d) method, which has the same structure as LM_6 in Figure 2. Li et al.[8] studied this pathway by photodissociation of nitrobenzene at 266 nm using the single-photon laser-induced fluorescence technique. They also calculated the PES for this pathway at the B3LYP/6-31G(d) level. Comparing their calculated results with ours, we find the two transition states TS(a) and TS(b) in their work should be the same ones as TS_9 confirmed by an IRC calculation in our work. LM_6 (C_6H_5ONO(a) in their work) and LM_7 (C_6H_5ONO(b) in their work) can transform into each other by TS_{10}, and both can dissociate to the $C_6H_5O + NO$ products.

The predicted dissociation energy for $C_6H_5O + NO$ relative to nitrobenzene is 23.6 kcal/mol with the G2M method and 21.7 kcal/mol using G3B3. These values may be compared with 22.5 kcal/mol relative to phenylnitrite predicted by G2M. The latter agrees well with the experimental bond dissociation energy of C_6H_5O-NO at 0 K, 20.0 ± 1.9 kcal/mol.[15]

2c. $C_6H_5NO_2 \rightarrow C_6H_4 + HONO$. This pathway was not observed in previous photodissociation and thermal decomposition experiments.[1−10] The predicted dissociation energy for this pathway is 76.1 kcal/mol by G2M and 76.4 kcal/mol using the G3B3 method. These values are close to the experimental heat of reaction at 0 K, 72.4 ± 5.0 kcal/mol, according to $\Delta_f H_0$(HONO) = −16.85 ± 0.32 kcal/mol,[21] $\Delta_f H_0(C_6H_4) = 110.2 \pm 5.0$ kcal/mol based on $\Delta_f H_{300}(C_6H_4) = 108.0 \pm 5.0$ kcal/mol,[22] and $\Delta_f H_0(C_6H_5NO_2) = 20.95 \pm 0.12$ kcal/mol evaluated above.

There are two possible channels to produce $C_6H_4 + HONO$; in the first channel nitrobenzene directly eliminates HONO via a 5-centered transition state TS_8 with a barrier of 78.6 kcal/mol. In the second channel, the reaction takes place via five isomers (including the most stable 2-nitrosophenol) and seven transition states, two of which are rather high as referred to above for isomerization reactions. Contributions from both channels to the thermal decomposition reaction are negligible as will be discussed later.

2d. $C_6H_5NO_2 \rightarrow C_6H_5NO + O$. Although this pathway is unimportant in the thermal decomposition reaction, it was observed by Galloway et al.[9] in the photodissociation nitrobenzene between 220 and 320 nm by vacuum-ultraviolet photoionization molecular-beam mass spectrometry and also by Kosmidis[5] and Clark et al.[23] using a time-of-flight mass spectrometer in the wavelength range 225−275 nm. They detected the triplet O atom, and not the excited O(^{1}D), as a product, suggesting that the fragmentation process may occur by a charge-transfer state, followed by intersystem crossing to a triplet manifold where the dissociation takes place.[5,9,23]

The predicted dissociation energy for this pathway is 93.1 kcal/mol by G2M and 92.1 kcal/mol using the G3B3 method; These values are close to the experimental heat of reaction at 0 K, 89.6 ± 1.3 kcal/mol, using $\Delta_f H_0(C_6H_5NO_2) = 20.95 \pm 0.12$ kcal/mol, $\Delta_f H_0(O) = 58.98$ kcal/mol,[21] and $\Delta_f H_0(C_6H_5NO) = 51.6 \pm 1.1$ kcal/mol determined by the C−N bond dissociation energy of C_6H_5-NO with 54.2 ± 0.5 kcal/mol at 0 K,[24] $\Delta_f H_0(C_6H_5) = 84.3 \pm 0.6$ kcal/mol,[22] and $\Delta_f H_0(NO) = 21.46 \pm 0.04$ kcal/mol.[21]

3. Rate Constants Calculations

3a. Decomposition of $C_6H_5NO_2$. As mentioned in the above section, there are four possible channels for dissociation of $C_6H_5NO_2$; however, the channel of $C_6H_5NO_2 \rightarrow C_6H_5NO + O$ is unimportant in the thermal decomposition reaction, therefore, we have carried out variational TST and RRKM calculations for the following three major reaction channels based on the PES and mechanisms presented in the preceding section.

$$C_6H_5NO_2 \xrightarrow{k_1} C_6H_5 + NO_2$$

$$\xrightarrow{k_2} C_6H_5O + NO$$

$$\xrightarrow{k_3} C_6H_4 + HONO$$

The geometries, vibrational frequencies, and rotational constants of the reactants and products are from the calculations by B3LYP/6-311G(d, p). The relative energies between the products and reactants are from the calculations using the G2M method listed in Table 1.

The rate constants for the dissociation reactions (k_1, k_2, k_3) have been calculated using the Variflex code.[25] For k_1 calculations, the minimum energy path (MEP) representing the barrierless dissociation process $C_6H_5NO_2 \rightarrow C_6H_5 + NO_2$ is obtained by calculating the potential curve along the reaction coordinate C−N of $C_6H_5NO_2 \rightarrow C_6H_5 + NO_2$, where the C−N bond length is stretched from the equilibrium value 1.481 to 6 Å with a step size of 0.2 Å, and each geometry with a fixed C−N bond length is fully optimized at the B3LYP/6-311G(d, p) level. The MEP is approximated with the Morse potential, $V(r) = D_e\{1 - \exp[-\beta (R - R_0)]\}^2$, where R is the reaction coordinate, R_0 is the equilibrium value, and D_e is the bond energy without zero-point energy corrections. The parameters of the Morse potential obtained by fitting the MEP are $R_0 = 1.481$, $\beta = 1.29$ Å^{-2}, and $D_e = 77.6$ kcal/mol, which was scaled slightly to the G2M value without ZPE-correction, respectively. In addition, the Lennard-Jones pairwise potential and the anisotropic potential (a potential anisotropy form assuming a bonding potential which is cylindrically symmetric with respect to each fragment) are also added together to form the final potential for the variational rate constant calculation by the Variflex code.[24] k_2 and k_3 are controlled by the well-defined TS_9 and TS_8, respectively.

The predicted high-pressure, first-order rate constants for the 3 decomposition reactions producing $C_6H_5 + NO_2$, $C_6H_5O + NO$ and $C_6H_4 + HONO$ in the temperature range 500−2000 K can be given by

$$k_1^{\infty} = 1.52 \times 10^{17} \exp[-37100/T]\ s^{-1}$$

$$k_2^{\infty} = 7.12 \times 10^{13} \exp[-31500/T]\ s^{-1}$$

$$k_3^{\infty} = 1.33 \times 10^{15} \exp[-40900/T]\ s^{-1}$$

To compare the theory with experiments, we have calculated the rate constants in the temperature range 500−2000 K under different experimental conditions. The Lennard-Jones (L−J) parameters for different bath gases are employed: Ar, $\sigma = 3.47$ Å, $\epsilon/k = 114$ K;[22] SF_6, $\sigma = 5.20$ Å, $\epsilon/k = 212$ K;[22] $C_6H_5NO_2$, $\sigma = 5.0$ Å, $\epsilon/k = 400$ K. These are derived from the critical temperature (713 K) and volume (309.5 cm^3/mol) using the formulas $\epsilon/k = 0.897T_c$ and $\sigma = 0.785\ V_c^{1/3}$.[26] The predicted values shown in Figure 3 for the conditions close to those employed experimentally are compared reasonably with experimental results cited in the Introduction. For example, for the conditions employed by Tsang and co-workers[3] using Ar as bath gas, the predicted rate expression $k_1 = 2.5 \times 10^{15}$

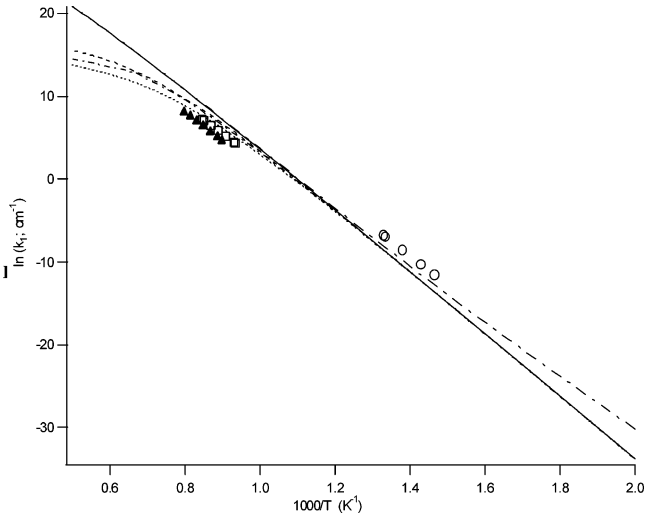

Figure 3. Dissociation rate constants of $C_6H_5NO_2 \rightarrow C_6H_5 + NO_2$. Experimental data: "○", data from ref 1; "□", data from ref 3; "▲", data from ref 2. Predicted values: solid line, the high-pressure limit; dotted curve, the rate constants with 200 Torr pure nitrobenzene; dashed curve, rate constants with Ar as bath gas at 2500 Torr; dash dotted curve, rate constants with 100 Torr SF_6; longer dash-dotted line, total dissociation rate constants in the high-pressure limit.

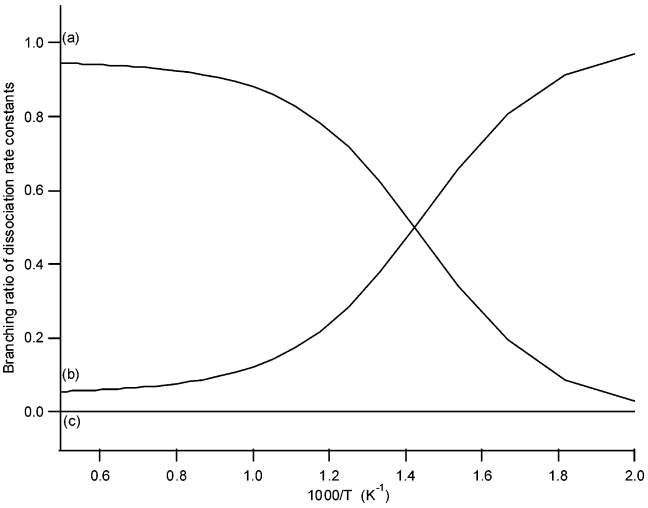

Figure 4. Calculated branching ratios for (a) $C_6H_5NO_2 \rightarrow C6H_5 + NO_2$, (b) $C_6H_5NO_2 \rightarrow C6H_5O + NO$, and (c) $C_6H_5NO_2 \rightarrow C6H_4 + HONO$ at 760 Torr Ar in the temperature range 500−2000 K.

$\exp[-32700/T]$ s^{-1} is in close agreement with their result, $k_1 = 1.9 \times 10^{15} \exp[-33700/T]$ s^{-1}. Similarly, for the decomposition studied by Matveev et al. in pure nitrobenzene at lower temperatures[1] where the contribution by k_2 becomes significant (vide infra), the theoretical result, $(k_1 + k_2) = 2.40 \times 10^{17} \exp[-37400/T]$ s^{-1}, is also in fair agreement with the experimental data $k_1 = 2.09 \times 10^{17} \exp[-(35900 \pm 716)/T]$ s^{-1}. Finally, the predicted expression, $k_1 = 1.70 \times 10^{15} \exp[-33200/T]$ s^{-1} for the same experimental conditions as employed by Gonzalez et al.[2] using the SF_6 bath gas, also agrees reasonably with the experimental data given by $k_1 = 3.16 \times 10^{15} \exp[-(35200 \pm 702)/T]$ s^{-1}.

Because of the lower energy barrier for the production of the phenoxy radical, its contribution is significant at temperatures below 850 K, as shown by the predicted branching ratios of the three product channels under the atmospheric pressure condition in Figure 4. As is evident from the figure, $k_3/(k_1 + k_2 + k_3)$ is negligibly small throughout the temperature range 500−2000 K; $k_1/(k_1 + k_2 + k_3)$ is approaching unity at $T > 850$ K. However, as T decreases from 850 to 500 K, $k_1/(k_1 + k_2 + k_3)$ decreases from 0.78 to 0.03, while that of reaction 2 increases from 0.22 to 0.97. Therefore, the $C_6H_5O + NO$ product path shows a competitively significant contribution to the decomposition of nitrobenzene at $T < 850$ K. Reaction 2 should accordingly account significantly for Matveev's products measured in the temperature range 683−753 K,[1] although experimentally it is difficult to differentiate $C_6H_5O + NO$ from $C_6H_5 + NO_2$, which react rapidly to give the former products as discussed below. The predicted rate constants in the low-pressure limit in the Ar bath gas at 500−2000 K can be given by

$$k_1^\circ = 9.69 \times 10^{105} \times T^{-25.6} \exp[-48200/T] \text{ cm}^3 \text{ mol}^{-1} \text{ s}^{-1}$$

$$k_2^\circ = 7.11 \times 10^{99} \times T^{-23.7} \exp[-44500/T] \text{ cm}^3 \text{ mol}^{-1} \text{ s}^{-1}$$

$$k_3^\circ = 1.16 \times 10^{101} \times T^{-25.8} \exp[-48900/T] \text{ cm}^3 \text{ mol}^{-1} \text{ s}^{-1}$$

3b. Reaction of C_6H_5 with NO_2. The rate constants for reactions C_6H_5 with NO_2 via the two distinct intermediates, $C_6H_5NO_2$ and C_6H_5ONO have been calculated in the temperature range 300−2000 K using argon as the bath gas according to the following scheme:

A. $C_6H_5NO_2$ path:

$$C_6H_5 + NO_2 \xrightarrow{k_{-1}} C_6H_5NO_2\,(+M)$$

$$\rightarrow C_6H_5NO_2^* \xrightarrow{k_{-2}} C_6H_5O + NO$$

$$\rightarrow C_6H_5NO_2^* \xrightarrow{k_{-3}} C_6H_4 + HONO$$

B. C_6H_5ONO path:

$$C_6H_5 + NO_2 \xrightarrow{k_{-4}} C_6H_5ONO(+M)$$

$$\rightarrow C_6H_5ONO^* \xrightarrow{k_{-5}} C_6H_5O + NO$$

Here "*" denotes internal excitation. The rate constants for the reaction via $C_6H_5NO_2$ have been calculated with the Variflex code[25] using the transition state and molecular parameters as employed for the forward $C_6H_5NO_2$ decomposition reaction discussed in the preceding section. For the reaction via C_6H_5-ONO, the potential energy curves for the formation and decomposition of the intermediate, $C_6H_5 + NO_2 \rightarrow C_6H_5ONO$ and $C_6H_5ONO \rightarrow C_6H_5O + NO$ were obtained by stretching the lengths of the C−O and O−N bonds in C_6H_5ONO with the step size of 0.2 Å from their equilibrium values to 5 Å, respectively. Each geometry with the fixed C−O or O−N bond length has been optimized at the B3LYP/6-311G(d, p) level. The minimum energy paths were approximated with the Morse potentials, whose parameters were obtained by fitting the calculated potential energy curves as before. For the association reaction $C_6H_5 + NO_2 \rightarrow C_6H_5ONO$, $\beta = 1.36$ Å^{-2} with $R_0 = 1.382$ Å and the D_e value was rescaled from 67.2 kcal/mol obtained at the B3LYP level to the calculated dissociation energy of $C_6H_5ONO \rightarrow C_6H_5 + NO_2$ by G2M without ZPE corrections. Similarly, for the decomposition reaction $C_6H_5ONO \rightarrow C_6H_5O + NO$, $\beta = 1.33$ Å^{-2} with $R_0 = 1.498$ Å, and the D_e value was rescaled from its DFT value (17.5 kcal/mol) to the calculated dissociation energy (see Table 1). For C_6H_5ONO reaction path, the isomerization between the LM_7 and LM_6 was ignored because the isomerization of C_6H_5O-NO by internal rotation of the ON group can be efficiently treated as a free rotor.

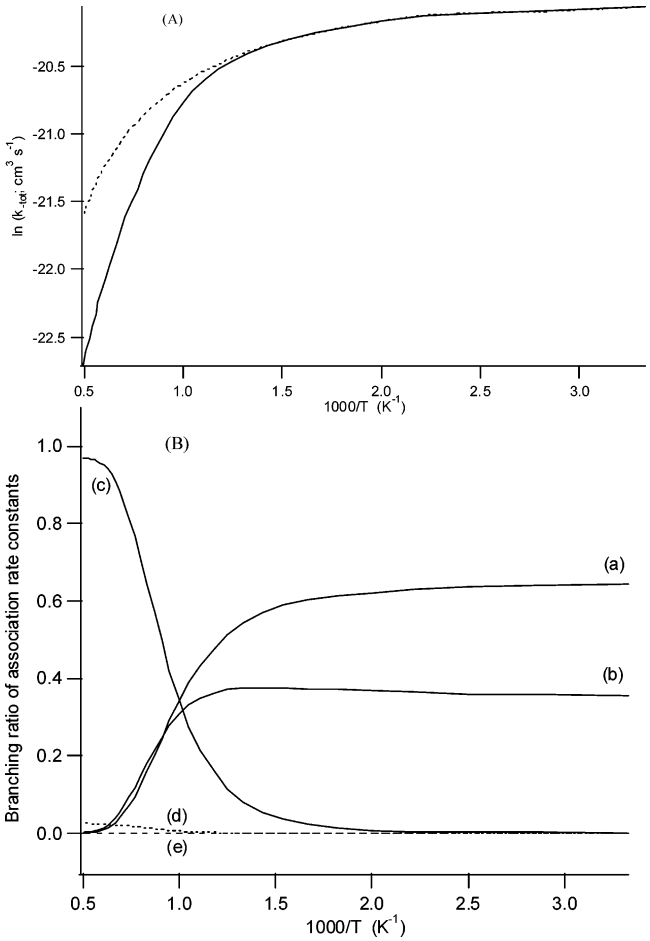

Figure 5. (A), Total association rate constants for $C_6H_5 + NO_2$ calculated at 760 Torr Ar (solid curve) and at the high-pressure limit (dotted curve) at temperatures 300−2000 K. (B), Calculated branching ratios for formation of (a) C_6H_5ONO, (b) $C_6H_5NO_2$, (c) $C_6H_5O + NO$ via C_6H_5ONO, (d) $C_6H_5O + NO$ via $C_6H_5NO_2$ and C_6H_5ONO (dotted line), and (e) $C_6H_4 + HONO$ via $C_6H_5NO_2$ (dashed line) at 760 Torr Ar in the temperature range 300−2000 K.

The total rate constant for the reaction of C_6H_5 with NO_2 is shown in Figure 5 A. Using the three parameter function, the total rate expression for the association reaction of the $C_6H_5 + NO_2$ is $k = 285 \times T^{-3.61} \exp[-1600/T]$ cm^3 molecule^{-1} s^{-1} at 760 Torr Ar pressure, $k = 3.4 \times 10^{-4} \times T^{-1.73} \exp[-680/T]$ cm^3 molecule^{-1} s^{-1} at the high-pressure limit, respectively. The branching ratios for the five channels for the bimolecular $C_6H_5 + NO_2$ reaction under atmospheric pressure are shown in Figure 5B. As shown in the Figure, at temperatures $T < 800$ K, the dominating processes are collisional deactivation producing (a) C_6H_5ONO and (b) $C_6H_5NO_2$ with branching ratios of 0.64 and 0.36, respectively. At temperature $T > 800$ K, the branching ratio for the formation of (c) $C_6H_5O + NO$ goes up rapidly from 0.08 to 0.97. The branching ratios for the product channels (d) $C_6H_5 + NO_2 \rightarrow C_6H_5NO_2^* \rightarrow C_6H_5O + NO$ and (e) $C_6H_5 + NO_2 \rightarrow C_6H_5NO_2^* \rightarrow C_6H_4 + HONO$ are both negligibly small. All phenoxy radical is formed primarily via phenylnitrite throughout the temperature range studied.

3c. Association of C_6H_5O with NO. The rate constants for the association reaction $C_6H_5O + NO (+M) \rightarrow C_6H_5ONO (+M)$ has also been calculated by the Variflex code[25] for comparison with available experimental data. The reaction was first studied in 1995 by our group[14] using the cavity ring-down method monitoring the decay of the C_6H_5O radical. The bimolecular rate constant determined in the temperature range 297−373 K at 40 Torr argon can be represented by $k (C_6H_5O + NO) = 10^{-12.12} \pm 0.0.24 \exp[(198 \pm 189)/T]$ cm^3 molecule^{-1} s^{-1}. In that work, C_6H_5ONO was shown to be the most likely and stable association product by RRKM calculations using the energetics and molecular parameters predicted at the MP4(SDQ)//HF/6-31G(d) level. Berho et al.[15] also studied the kinetics of the association reaction using a flash photolysis technique coupled with UV absorption spectroscopy. They obtained $k (C_6H_5O + NO) = (1.65 \pm 0.10) \times 10^{-12}$ cm^3 molecule^{-1} s^{-1} in the temperature range 280−328 K at atmospheric N_2 pressure. By B3LYP/6-31G(d) calculations, they also confirmed that C_6H_5-ONO was the principal association product. In addition, Platz et al.[16] studied the association reaction using pulse photolysis and FTIR technique; they reported $k (C_6H_5O + NO) = (1.88 \pm 0.16) \times 10^{-12}$ cm^3 molecule^{-1} s^{-1} at 296 K in the presence of 750 Torr SF_6. These experimental data are summarized in Figure 6.

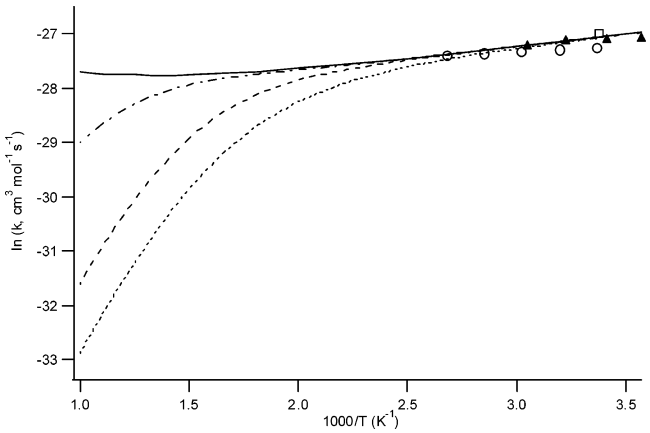

Figure 6. Association rate constants of $C_6H_5O + NO \rightarrow C_6H_5ONO$. Experimental data: "○", data from ref 14; "▲", data from ref 15; "□", data from ref 16. Predicted results: solid line, the high-pressure limit rate constants at 280−1000 K; dotted curve, rate constants with 40 Torr Ar at 297−1000 K; dashed curve, rate constants at 760 Torr Ar and 280−1000 K; dash dotted curve, rate constants with SF_6 as bath gas at 750 Torr in the temperature range 296−1000 K.

The predicted rate constants $k (C_6H_5O + NO)$ are compared with experimental data in Figure 6 using the same experimental conditions as employed by Yu et al.,[14] Berho et al.,[15] and Platz et al.[16] cited above. The temperature range has been extended to 1000 K in the calculation using the same L−J parameters given for $C_6H_5NO_2$ collision with Ar and SF_6. Those of N_2 are $\sigma = 3.68$ Å, $\epsilon/k = 91.5$ K.[15] For average stepsize collisional deactivation, $\langle \Delta E \rangle_{down}$ are 400 cm^{-1} for Ar,[27,28] 300 cm^{-1} for N_2 by averaging the reference data of 200−400 cm^{-1},[27−29] and 2200 cm^{-1} for SF_6 assumed by this work according to the reference data of 1000 cm^{-1} for the smaller reaction system of $OH + CO$,[27] respectively, throughout the temperature range studied. The predicted rate expression $k (C_6H_5O + NO) = 2.65 \times 10^{-13} \exp[+570/T]$ cm^3 molecule^{-1} s^{-1} for Yu's experimental condition,[14] $k (C_6H_5O + NO) = (1.93-1.52) \times 10^{-12}$ cm^3 molecule^{-1} s^{-1} for Berho's condition,[15] and $k (C_6H_5O + NO) = 1.77 \times 10^{-12}$ cm^3 molecule^{-1} s^{-1} for Platz's condition,[16] are all in good agreement with the experimental data as shown in Figure 6. The high-pressure-limit rate constant for $C_6H_5O + NO$ in the temperature range 300−1000 K, $k^\infty (C_6H_5O + NO) = 5.99 \times 10^{-13} \exp[+310/T]$ cm^3 molecule^{-1} s^{-1}, is also shown in the Figure. At 298 K, the value $k^\infty (C_6H_5O + NO) = 1.80 \times 10^{-12}$ cm^3 molecule^{-1} s^{-1} is in exact agreement with that predicted by Berho et al. based on an RRKM calculation.[15]

Conclusions

The energies of nitrobenzene, its eight isomers, and 11 transition states have been calculated with the G2M (RCC, MP2) method based on the optimized structures at the B3LYP/6-311G-(d, p) level. The dissociation energies of nitrobenzene for the four pathways have also been predicted with the G3B3 method; they are in reasonable agreement with those predicted by G2M and experimental data. The dissociation producing $C_6H_5 + NO_2$ is the main channel with its branching ratio > 0.78 above 850 K. When the temperature decreases from 850 to 500 K, the second dissociation path producing $C_6H_5O + NO$ via the C_6H_5-ONO intermediate becomes competitive with its branching ratio increasing from 0.22 to 0.97. The third dissociation pathway, $C_6H_5NO_2 \rightarrow C_6H_4 + HONO$, is negligibly small throughout the temperature studied, 500−2000 K. The predicted dissociation rate constant for $C_6H_5NO_2 \rightarrow C_6H_5 + NO_2$ is in good agreements with previous experimental data.

We have also calculated the rate constants for the association of C_6H_5 with NO_2. Three key pathways have been identified to produce (a) C_6H_5ONO and (b) $C_6H_5NO_2$ by association/collisional stabilization and (c) $C_6H_5O + NO$ by disproportionation via the C_6H_5ONO intermediate in the temperature range 300−2000 K at 760 Torr Ar pressure. At temperatures $T <$ 800 K, the branching ratios for pathways a and b have been predicted to be 0.64 and 0.36, respectively. At temperatures $T >$ 800 K, the branching ratio for c increases rapidly from 0.08 to 0.97. The two other paths, (d) $C_6H_5 + NO_2 \rightarrow C_6H_5NO_2^* \rightarrow C_6H_5O + NO$ and (e) $C_6H_5 + NO_2 \rightarrow C_6H_5NO_2^* \rightarrow C_6H_4 + HONO$, have been found to be negligibly small throughout the temperature range calculated. Finally, the association rate constant for $C_6H_5O + NO \rightarrow C_6H_5ONO$ has also been predicted; the result is in good agreement with existing experimental data.

Acknowledgment. We are grateful to the support of this work from the Basic Energy Sciencies, Department of Energy, under Contract DE-FG02-97-ER14784, and Cherry L. Emerson Center for Scientific Computation of Emory University for the use of its resources, which are in part supported by a National Science Foundation Grant (CHE-0079627) and an IBM shared University Research Award. M.C.L. also acknowledges the support from the National Science Council of Taiwan for a Distinguished Visiting Professorship at National Chiao Tung University in Hsichu, Taiwan. S.X. is also thankful for the support from Cherry L. Emerson Center for Scientific Computation of Emory University for a Cherry L. Emerson Visiting Fellowship.

References and Notes

(1) Matveev, V. G.; Nazin, G. M. *Bull. Acad. Sci. USSR Div. Chem. Sci.* **1975**, *24*, 697.

(2) Gonzalez, A. C.; Lamon, C. W.; McMillen, D. F.; Golden, D. M. *J. Phys. Chem.* **1985**, *89*, 4809.

(3) Tsang, W.; Robaugh, D.; Mallard, W. G. *J. Phys. Chem.* **1986**, *90*, 5968.

(4) Marshall, A.; Clark, A.; Jennings, R.; Ledingham, K. W. D.; Singhal, R. P. *Int. J. Mass Spectrom. Ion Processes* **1992**, *112*, 273.

(5) Kosmidis, C.; Ledingham, K. W. D.; Clark, A.; Marshall, A.; Jennings, R.; Sander, J.; Singhal, R. P. *Int. J. Mass Spectrom. Ion Processes* **1994**, *135*, 229.

(6) Kosmidis, C.; Ledingham, K. W. D.; Kilic, H. S.; McCanny, T.; Singhal, R. P.; Langley, A. J.; Shaikh, W. *J. Phys. Chem. A* **1997**, *101*, 2264.

(7) Daugey, N.; Shu, J.; Bar, I.; Rosenwaks, S. *Appl. Spectrosc.* **1999**, *53*, 57.

(8) Li, Y.-M.; Sun, J.-L.; Yin, H.-M.; Han, K.-L.; He, G.-Z. *J. Chem. Phys.* **2003**, *118*, 6244.

(9) Galloway, D. B.; Bartz, J. A.; Huey, L. G.; Crim, F. F. *J. Chem. Phys.* **1993**, *98*, 2107.

(10) Galloway, D. B.; Glenewinkel-Meyer, T.; Bartz, J. A.; Huey, L. G.; Crim, F. F. *J. Chem. Phys.* **1994**, *100*, 1946.

(11) Takezaki, M.; Hirota, N.; Terazima, M.; Sato, H.; Nakajima, T.; Kato, S. *J. Phys. Chem. A* **1997**, *101*, 5190.

(12) Glenewinkel-Meyer, T.; Grim, F. F. *J. Mol. Struct. (THEOCHEM)* **1995**, *337*, 209.

(13) Polasek, M.; Turecek, F.; Gerbaux, P.; Flammang, R. *J. Phys. Chem. A* **2001**, *105*, 995.

(14) Yu, T.; Mebel, A. M.; Lin, M. C. *J. Phys. Org. Chem.* **1995**, *8*, 47.

(15) Berho, F.; Caralp, F.; Rayez, M.-T.; Lesclaux, R.; Ratajczak, E. *J. Phys. Chem. A* **1998**, *102*, 1.

(16) Platz, J.; Nielsen, O. J.; Wallington, T. J.; Ball, J. C.; Hurley, M. D.; Straccia, A. M.; Schneider, W. F. *J. Phys. Chem. A* **1998**, *102*, 7964.

(17) Mebel, A. M.; Morokuma, K.; Lin, M. C. *J. Chem. Phys.* **1995**, *103*, 7414.

(18) Baboul, A. G.; Curtiss, L. A.; Redfern, P. C. *J. Chem. Phys.* **1999**, *110*, 7650.

(19) Frisch, M. J.; Trucks, G. W.; Schlegel, H. B.; Scuseria, G. E.; Robb, M. A.; Cheeseman, J. R.; Zakrzewski, V. G.; Montgomery, J. A., Jr.;; Stratmann, R. E.; Burant, J. C.; Dapprich, S.; Millam, J. M.; Daniels, A. D.; Kudin, K. N.; Strain, M. C.; Farkas, O.; Tomasi, J.; Barone, V.; Cossi, M. C.; R.; Mennucci, B.; Pomelli, C.; Adamo, C.; Clifford, S.; Ochterski, J.; Petersson, G. A.; Ayala, P. Y.; Cui, Q.; Morokuma, K.; Malick, D. K.; Rabuck, A. D.; Raghavachari, K.; Foresman, J. B.; Cioslowski, J.; Ortiz, J. V.; Baboul, A. G.; Stefanov, B. B.; Liu, G.; Liashenko, A.; Piskorz, P.; Komaromi, I.; Gomperts, R.; Martin, R. L.; Fox, D. J.; Keith, T.; Al-Laham, M. A.; Peng, C. Y.; Nanayakkara, A.; Gonzalez, C.; Challacombe, M.; Gill, P. M. W.; Johnson, B.; Chen, W.; Wong, M. W.; Andres, J. L.; Gonzalez, C.; Head-Gordon, M.; Replogle, E. S.; Pople, J. A. *Gaussian 98, Revision A.7.* Gaussian, Inc.: Pittsburgh, PA, 2003.

(20) Amos, R. D.; Bernhardsson, A.; Berning, A.; Celani, P.; Cooper, D. L.; Deegan, M. J. O.; Dobbyn, A. J.; Eckert, F.; Hampel, C.; Hetzer, G. K.; P. J.; Korona, T.; Lindh, R.; Lloyd, A. W.; McNicholas, S. J.; Manby, F. R.; Meyer, W.; Mura, M. E.; Nicklass, A.; Palmieri, P.; Pitzer, R.; Rauhut, G.; Schutz, M.; Schumann, U.; Stoll, H.; Stone, A. J.; Tarroni, R.; Thorsteinsson, T.; Werner, H.-J. *MOLPRO, version 98.1*; University of Birmingham: Birmingham, U.K., 1998.

(21) Chase, M. W. *NIST-JANAF Thermchemical Tables*; 4th ed.; AIP: Woodbury, NY, 1998.

(22) Davico, G. E.; Bierbaum, V. M.; DePuy, C. H.; Ellison, G. B.; Squires, R. R. *J. Am. Chem. Soc.* **1995**, *117*, 2590.

(23) Clark, A.; Kosmidis, C.; Ledingham, K. W. D.; Marshall, A.; Sander, J.; Singhal, R. P.; Campbell, M. *J. Phys. B* **1993**, *26*, L665.

(24) Park, J.; Dyakov, I. V.; Mebel, A. M.; Lin, M. C. *J. Phys. Chem. A* **1997**, *101*, 6043.

(25) S. J. Klippenstein, A. F. W.; R. C. Dunbar, D. M. Wardlaw, S. H. Robertson,. *Variflex*, **1999.**

(26) Mourits, F. M.; Rummens, F. H. A. *Can. J. Chem.* **1977**, *55*, 3007.

(27) Zhu, R. S.; Diau, E. G. W.; Lin, M. C.; Mebel, A. M. *J. Phys. Chem. A* **2001**, *105*, 11249.

(28) Zhu, R. S.; Lin, M. C. *J. Chem. Phys.* **2003**, *118*, 4094.

(29) Golden, D. M.; Smith, G. P.; McEwen, A. B.; Yu, L. C.; Eiteneer, B.; Frenklach, M.; Vaghjiani, G. L.; Ravishankara, A. R.; Tully, F. P. *J. Phys. Chem.* **1998**, *102*, 8598.